Phase-Separation Processes and Self-Organization of Textures in the Biphase Region of Thermotropic Liquid Crystalline Poly(4,4′-dioxy-2,2′-dimethylazoxybenzene−dodecanedioyl). 2. A Study of the Isothermal Conditions

Akemi Nakai,† Wei Wang, and Takeji Hashimoto*

Department of Polymer Chemistry, Graduate School of Engineering, Kyoto University, Kyoto 606-01, Japan

Alexandre Blumstein

Polymer Science Program, Department of Chemistry, University of Massachusetts Lowell, Lowell, Massachusetts 01854

Received July 31, 1995; Revised Manuscript Received April 29, 1996[⊗]

ABSTRACT: The isothermal phase-separation process and the self-organization of textures in the biphase region of a thermotropic liquid crystalline polyester were investigated *in situ* by using polarizing light microscopy. When the test temperature was rapidly raised from room temperature to the temperature corresponding to the biphase region (T-jump) or rapidly lowered from a temperature corresponding to the isotropic phase to that corresponding to the biphase region (T-drop), the phase separation occurs as a consequence of chain segregation according to the chain length: the chain species shorter than the average length gradually separate from the anisotropic phase to form the isotropic phase. The phase-separated textures transiently formed in the biphase region depend strongly on the thermal processes: in the case of the T-jump the coarsening of texture involves the diffusion−coalescence of isotropic drops in the anisotropic matrix, while in the case of the T-drop it involves the diffusion−coalescence of anisotropic drops in the isotropic matrix. For both cases growth of the radius of the drop R with the annealing time t obeys approximately the same power law, $R(t) \sim t^{1/3}$, over the time scale covered in this experiment. The coarsening mechanism is discussed in the text.

Introduction

For thermotropic main-chain liquid crystalline (LC) polymers, chemical heterogeneity, such as (i) the sequence distribution of rigid segments and their compositional variation and (ii) polydispersity of molecular mass (or chain length), is the origin of polydispersity in chain flexibility (*polyflexibility*). They are the main factors making the anisotropic−isotropic phase transition of such polymers more complex than that of low molecular weight liquid crystals.[1−12] A biphase region, wherein the anisotropic liquid phase coexists with the isotropic liquid phase, is developed transiently during the nematic−isotropic transition. For thermotropic LC polymers, the biphase region exists in a certain temperature interval even at thermal equilibrium. Formation of the biphase is ascribed to the partitioning of molecules with different chain flexibilities between the two phases.[1−12] For various statistical LC copolyesters, a broad biphase region was detected[1,2] and its formation was primarily explained by the polyflexibility, or more precisely by a polydispersity, of persistence lengths (factor i).[1,3] In contrast, the biphase behavior of the LC polymers with a chemically more regular structure appears in a somewhat narrower temperature interval, because it is primarily ascribed to the polyflexibility due to the polydispersity in molecular mass (factor ii).[4−12] In such LC polymers, macromolecules are partitioned within the isotropic and anisotropic phases according to their chain length; namely, a fraction of shorter chains cannot be incorporated into the nematic phase and is expelled from the nematic phase to form isotropic domains in which the molecules are expected to be essentially in a random coil conformation. On the other hand, another fraction of relatively longer chains remains in the anisotropic phase with an extended-chain conformation.

In our preceding paper[12] we reported on our experimental results concerning the phase-separation process and the self-organization of textures in the biphase region, obtained in the heating and cooling cycles, for a LC polyester, poly(4,4′-dioxy-2,2′-dimethylazoxybenzene−dodecanedioyl) (DDA-9). For DDA-9, the phase separation occurs as a consequence of chain segregation according to the chain length (factor ii). Obviously, the average molecular weight in the anisotropic phase is higher than that in the isotropic phase, as discussed in detail in our preceding paper.[12]

Further, we are intrigued by the phase-separated texture and process in the biphase region during the heating or cooling process.[12] For example, when a film sample was heated from a temperature corresponding to the pure anisotropic phase to that corresponding to the biphase, we observed that the short molecular species separated gradually from the anisotropic phase and formed isotropic regions or drops dispersed in the anisotropic matrix. The fraction of such drops increases with increasing temperature, leading to formation of an anisotropic network. When the temperature increased further, an increasing number of shorter chain species separated from the anisotropic phase and then the anisotropic network gradually broke up to form isolated anisotropic fragments in an isotropic matrix, before the total disappearance of the anisotropic phase. In contrast, when the test temperature decreased from the pure isotropic phase to the biphase, we observed first a quick anisotropization in the whole-sample space. After

† Present address: Department of Home Economics, Kyushu Women's Junior College, 1-1 Jiyugaoka, Yawatanishi, Kitakyushu 807, Japan.

[⊗] Abstract published in *Advance ACS Abstracts,* June 15, 1996.

the anisotropization, many anisotropic drops formed in the isotropic medium. In this case, the short-chain species form an isotropic medium as a consequence of a quick chain segregation. The short-chain species trapped in the anisotropic drops may be further expelled from the anisotropic drops into the isotropic matrix. The coalescence of the anisotropic drops leads to coarsening of the phase-separated texture. As temperature is lowered, the fraction of anisotropic drops increases, leading to a percolated thin network of isotropic liquid in a nematic medium.

These experimental results indicate clearly that the athermal conditions used are beneficial to qualitative studies of phase transition and the changes in structure occurring during the transition. However, the experimental conditions are not suitable for quantitative studies of the mechanism underlying the self-organization process in the biphase region, because the observed structural changes with temperature depend on the time scale of observation, and further, the temperature change alters the fractions of anisotropic and isotropic phases.

In this work we investigate the isothermal phase-separation process of DDA-9 in the biphase at a given temperature after rapidly changing the temperature from that corresponding to a pure anisotropic phase to that corresponding to the biphase (T-jump) or from that corresponding to a pure isotropic phase to that corresponding to the biphase (T-drop). Through the T-jump or T-drop processes, we can thus obtain two different biphase systems: one composed of isotropic drops in an anisotropic medium and the other composed of anisotropic drops in an isotropic medium. It is of interest to compare the phase-separation processes and the self-organization of textures occurring in both systems for the same polyester. To our best knowledge, there is no study on the coarsening mechanism of two systems composed of isotropic drops in the anisotropic matrix and of anisotropic drops in the isotropic matrix in the biphase region of the same LC polyester through the T-jump or T-drop processes.

Experimental Section

The DDA-9 used is the same as that used in the previous study.[12] It has a number-average molecular weight $\overline{M}_n = 2 \times 10^4$ and a polydispersity $\overline{M}_w/\overline{M}_n = 2.7$, which was determined by gel permeation chromatography (Waters GPC 150 °C with an RI detector) in chloroform at 40 °C. The yellow solid sample was dried in vacuum for 1 day at room temperature. Film specimens used for optical microscopy were prepared by pressing a small sample of the polymer between two clear glass slides on a heating stage preset to 167 °C which is approximately 5 °C higher than its clearing temperature.[12] A typical thickness of the film specimens is 20 μm. The specimens were annealed at 167 °C for 1 h to eliminate previous thermal history.

Previous study[12] shows that the biphase exists between 143 and 162 °C on heating and between 151 and 128 °C on cooling. Here it should be pointed out that the width of this biphase is not an equilibrium one as studied in ref 7. For the T-jump experiment, the specimen was first quenched to room temperature. The anisotropization occurred during the quenching process. The T-jump was then conducted by placing the quenched specimen on the heating stage preset at 148 °C. For the T-drop experiment, the specimen was quenched directly from 167 to 145 °C on the heating stage. The test temperatures were chosen in order to avoid the effect of the transesterification of DDA-9.[13]

The phase-separation process in the biphase region was observed *in situ* by a polarizing light microscope (PLM; Nikon Optiphot-Pol) with crossed polarizers between which a red plate having a retardation of 530 nm was inserted and with a heating−cooling stage (Linkam Th-600). One of the advantages in using a red plate is that it facilitates differentiation between isotropic areas and air bubbles.[12] In order to determine the fraction of one phase and the average size of a certain drop, the micrographs were first digitized by using a scan program (Apple Scan) and then the digitized data were analyzed by using image and analysis programs (NIH Image 1.53 and Adobe Photoshop 2.5).

Experimental Results

Before we present the experimental results, we indicate below why in this experiment we directly determined some quantities reflecting the phase-separation process from microscopy rather than from scattering. The main reasons are (i) the strong optical contrast attainable between isotropic and anisotropic phases under crossed polarizers, which makes our real-space observation easy, and also (ii) due to various ordering mechanisms being able to be directly studied under the microscope. The fact that the domain growth is very rapid, so that its scattering quickly degenerates into very small scattering angles where quantitative scattering analyses become difficult, also favors the real-space analysis. Scattering is a traditional method for studying the phase-separation processes in mixtures of polymers or other materials. However, it should be noted that the scattering data alone cannot determine detail mechanisms occurring in the processes.

A. Processes of Self-Organization via Phase Separation Induced by a T-Jump. A set of PLM micrographs in Figure 1 shows the isothermal phase-separation process and the self-organization of textures occurring at 148 °C. All the micrographs were taken from the same area. The red areas in the micrographs show the isotropic phase, while the bright areas normally having yellow or green color represent the anisotropic phase. From these and some other micrographs (not shown here), we can directly determine a number-average density of isotropic drops ρ_I, the fraction of the area of the isotropic phase x_I, and an interface length between the anisotropic and isotropic phases L. The average radius of isotropic drops R_I, was approximately determined according to $R_I = (S/\pi)^{1/2}$ where S is the average area of individual isotropic drops. The errors of these quantities measured are about 10%. The plots of these quantities as a function of the annealing time t (i.e., the time after the T-jump) are shown in Figure 2 where the experimental data are shown by symbols. The figure also includes some straight lines for possible interpretations of mechanisms underlying the self-organization processes in the system, as will be discussed in section A in the Discussion.

At first it should be noted that these quantities are obtained with two-dimensional (2D) images. However, the real structure observed by PLM has three-dimensional (3D) features, even in the case when the drop size is larger than the film thickness. The 3D feature of the structure can be easily visualized if one considers the curvature of the interface. However, for simplicity we ignored these intricate 3D features in discussing the quantities ρ_I, R_I, x_I, and L obtained from the micrographs; that is, we assume that all the interfaces are normal to the film surface. It should also be noted that, among the four quantities analyzed, only two are independent, since there are the following two relationships among them:

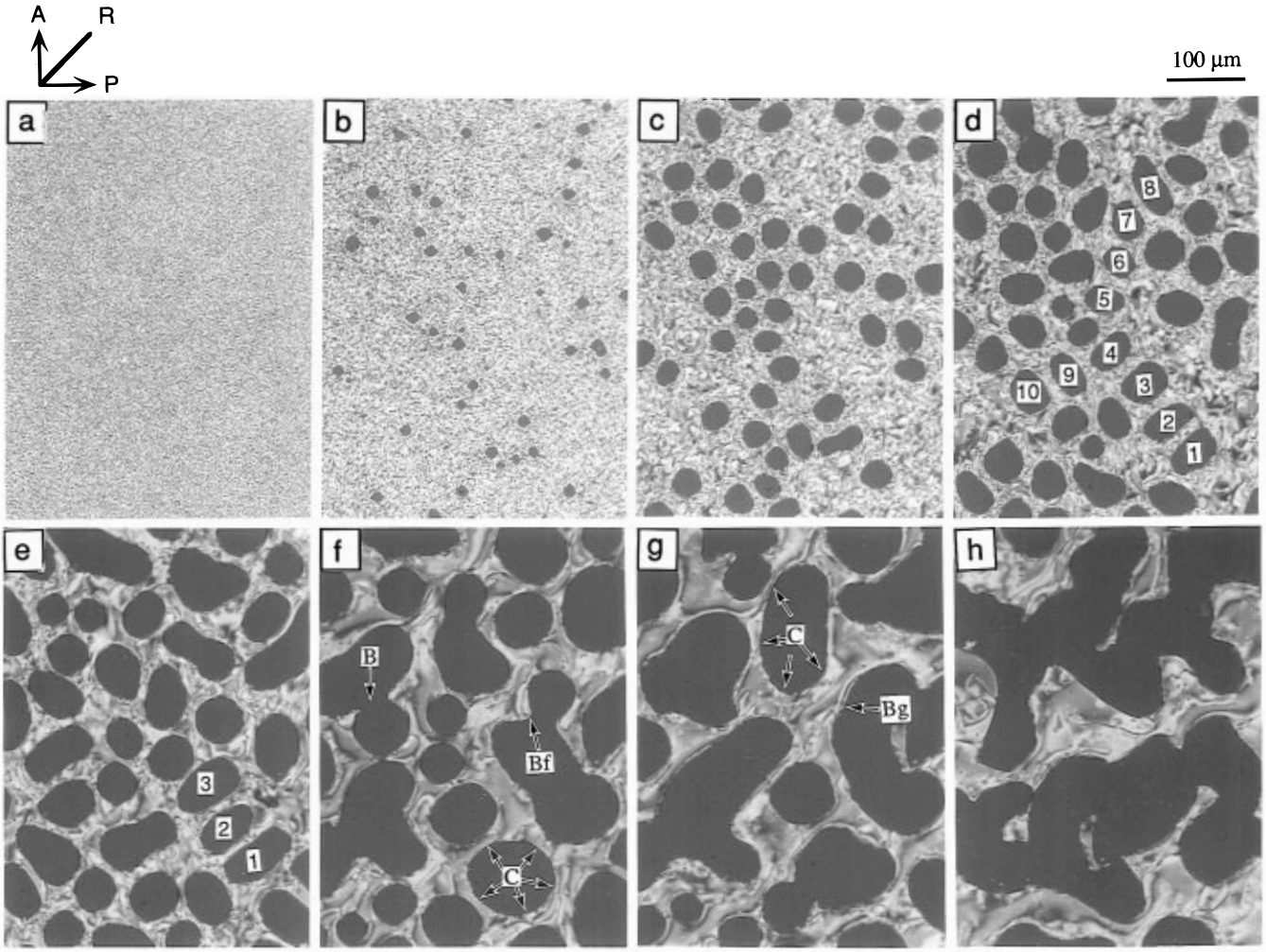

Figure 1. PLM micrographs showing the phase-separation process and the self-organization of textures of a fresh DDA-9 film specimen at 148 °C through the T-jump process. (a) shows the vitrified liquid crystal or crystalline structure of DDA-9 at room temperature. (b−h) show the time evolution of the phase-separated texture of DDA-9 at 148 °C: (b) $t = 20$ s; (c) $t = 60$ s; (d) $t = 120$ s; (e) $t = 300$ s; (f) $t = 900$ s; (g) $t = 1800$ s; (h) $t = 3600$ s. t is the time spent after the T-jump. These micrographs are obtained from the same area of the same sample.

$$x_I(t) \sim \rho_I(t) R_I^2(t) \quad (1)$$

$$L(t) \sim \rho_I(t) R_I(t) \quad (2)$$

For the sake of consistency of the image analysis, all four quantities are shown in Figure 2. The above equations are valid for the 2D structure and before significant domain impingement takes place.

Let us now discuss the data obtained from Figure 1 and those analyzed in Figure 2. Figure 1a shows a texture formed by quenching a DDA-9 specimen from 167 °C to room temperature. The specimen has a structure composed of vitrified nematic phase and/or crystalline phase. When the temperature was jumped to 148 °C, an isotropic phase forms in the anisotropic matrix, as shown in panels b and c of Figure 1. Correspondingly, the four quantities ρ_I, R_I, x_I, and L increase rapidly with t at $t < 40$ s, as shown in Figure 2. From Figure 1c−e we can see that the number of the isotropic drops does not change significantly but their size increases with t. These changes are reflected in Figure 2 such that ρ_I reaches a constant value but R_I, x_I, and L increase continuously with t at 40 s $< t <$ 300 s. In the time period of $t > 300$ s, the coalescence of the isotropic drops is shown in Figure 1e−h. The coalescence leads to different relationships of the four quantities with time: ρ_I and L decrease (Figure 2a and d), x_I reaches a constant value of ∼0.55 (Figure 2c), and R_I increases continuously (Figure 2b). These changes in different time intervals reflect different mechanisms of phase separation and self-organization, which will be discussed in section A in the Discussion.

B. Processes of Self-Organization via Phase Separation Induced by a T-Drop. When the specimen was quenched from 167 (fully isotropic state) to 145 °C (biphase region), the phase-separation process occurred in the biphase region, and the self-organization of textures occurring are shown by a set of PLM micrographs in Figure 3. As we did in Figure 1, we have directly determined the number-average density of anisotropic drops ρ_A and the fraction of the area of the anisotropic phase x_A from these and additional micrographs (not shown here). The average size of anisotropic drops R_A was approximately determined from the area S occupied by individual anisotropic drops according to $R_A = (S/\pi)^{1/2}$. The errors of these quantities measured are about 10% in this case too. It should be also noted that among the three quantities only two are independent, since $x_A(t) \sim \rho_A(t) R_A^2(t)$. The plots of these quantities with annealing time t (time elapsed after T-drop) are shown in Figure 4. The plot of L(t) vs t was omitted, simply because this quantity is given by $L_A(t) \sim \rho_A(t) R_A(t)$. The figure also includes some straight

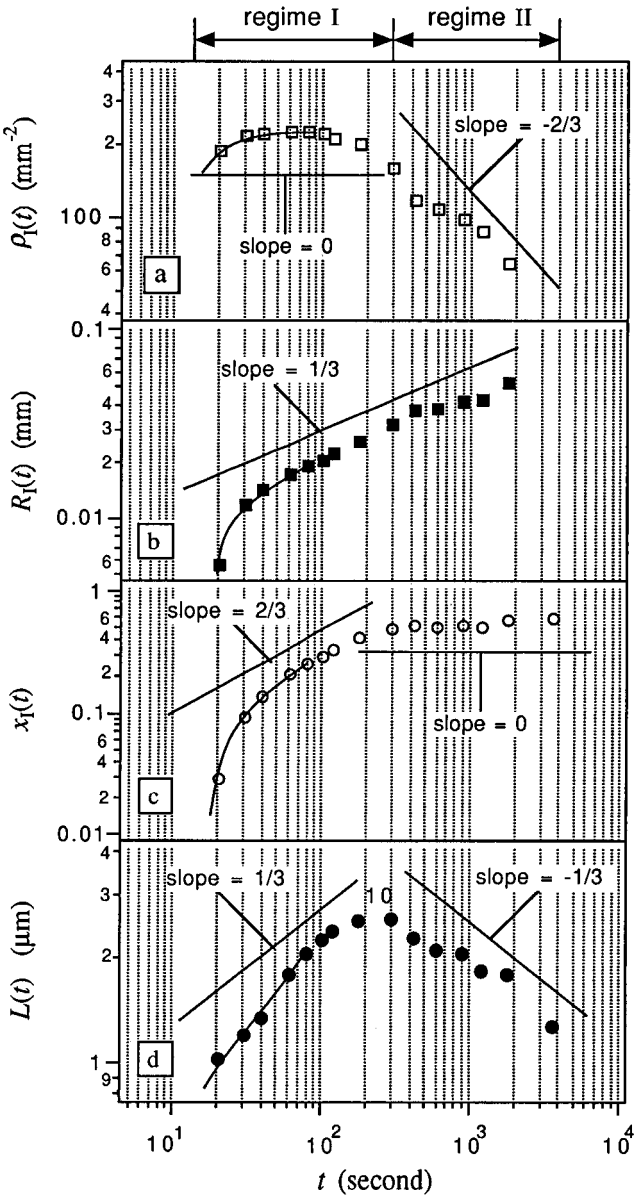

Figure 2. Plots of ρ_I, R_I, x_I and L with annealing time t. These quantities are determined from the micrographs, some of which are shown in Figure 1. The solid lines in regime I are drawn for a visual guide.

lines for possible interpretations of mechanisms underlying the self-organization process in the system, as will be discussed in section B in the Discussion.

Figure 3a shows a pure isotropic phase of a DDA-9 film specimen treated at 167 °C for 1 h. When the specimen was quenched to 145 °C, a phase-separated texture composed of very many small anisotropic drops in the isotropic matrix was developed, as shown in Figure 3b. From panels b to h in Figure 3 we see that anisotropic drops coalesced, leading to the decrease of their number (Figure 4a) but the increase of their size (Figure 4b). However, the measured results shown in Figure 4c show that x_A decreases at first with t and then reaches a constant value of about 0.63 at about 300 s. We will discuss the mechanism of the phase separation and the self-organization of texture in section B in the Discussion.

It is striking to note important differences between the time evolution of R_A and that of R_I: (i) the T-drop process generates an extremely large number of small anisotropic droplets compared with the T-jump process, which develops a smaller number of larger isotropic drops, as is obvious by comparing the time change in Figure 1a−c with that in Figure 3a−c, and (ii) the growth behavior of R_A itself is different from that of R_I, as is obvious by comparing Figure 2b with Figure 4b.

Discussion

A. Mechanisms of Self-Organization via Phase Separation Induced by a T-Jump. When the temperature was jumped to 148 °C, the phase separation occurred in the biphase region of DDA-9. This phase separation is driven by the chain segregation: a fraction of shorter chains in the LC phase with nematic-to-isotropic transition temperatures lower than 148 °C loses their extended-chain conformation required for being incorporated into the nematic phase. These shorter chains separate from the anisotropic matrix to form an isotropic phase, as shown in Figure 1b−h (red drops or domains).

Here we summarize an overall trend in the self-organization process showing in Figure 1. After the T-jump into the biphase region, a large number of small isotropic drops are formed in the anisotropic liquid matrix, as shown in Figure 1b. Only the drops whose size is greater than 10 μm are clearly discernible in the micrograph, though there must be a large number of smaller drops undetectable under microscope. These drops grow with time as shown in Figure 1b−e and eventually form a percolated network of an anisotropic phase in an isotropic matrix, as shown in Figure 1e−h. The network grows with dynamical self-similarity.[14,15] The time evolution of the structure may be divided into two regimes, judging from the results shown in Figure 2: regime I at $t < 300$ s (the corresponding structure change being shown in the micrographs a−d in Figure 1) and regime II at $t \gtrsim 300$ s (the corresponding one in the micrographs e−h in Figure 1).

We now attempt to give *very qualitative* interpretations on the data in each regime. Trends in time evolution of various structural quantities are qualitatively analyzed in terms of power laws below. However, we do not intend to claim the power laws and their exponents are quantitatively correct. More rigorous analyses are left for future studies.

Regime I. In regime I, the number-average density of isotropic drops $\rho_I(t)$ tends to increase with t to an approximately constant value toward the end of regime I, as shown in Figure 2a. Accordingly the average radius of the drops $R_I(t)$ increases with t, reaching an asymptotic power law behavior *approximately* given by

$$R_I(t) \sim t^{1/3} \tag{3}$$

toward the end of regime I, as shown in Figure 2b, and the power law tends to extend over regime II, as will be discussed later. From eq 1 together with the results shown in Figure 2a−b, it follows that the growth rate of $x_I(t)$ is slowed down with t, reaching an asymptotic behavior approximately given by

$$x_I(t) \sim t^{2/3} \tag{4}$$

toward the end of regime I, which is consistent with the experimental result shown in Figure 2c. Similarly from eq 2 together with the results shown in Figure 2a and b, the growth rate of $L(t)$ is slowed down with t, reaching asymptotically a behavior approximately given by

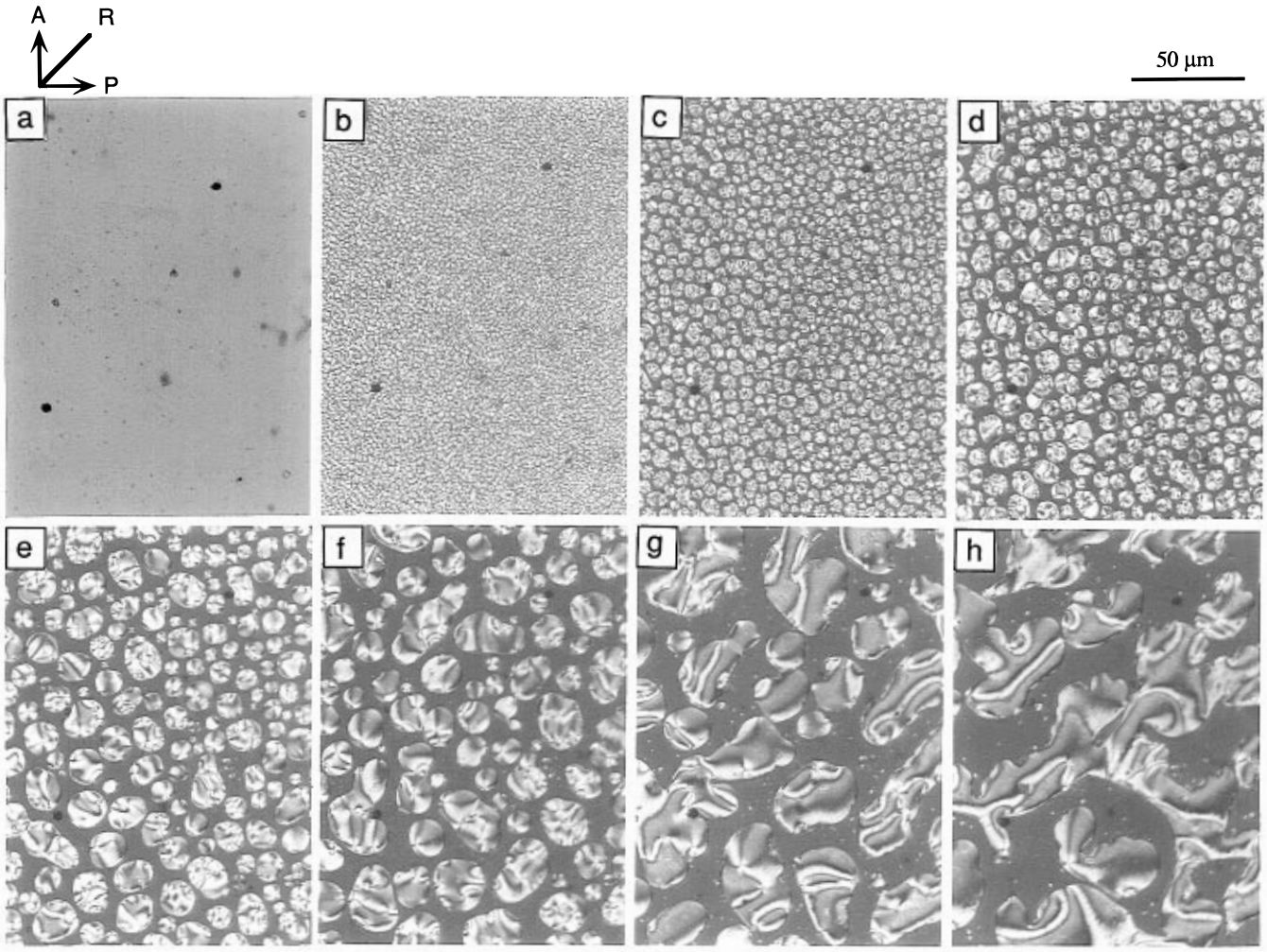

Figure 3. PLM micrographs showing the phase-separation process and the self-organization of the textures of a fresh DDA-9 film specimen at 145 °C through the T-drop process. (a) shows the isotropic state of the DDA-9 specimen at 167 °C. (b−h) show the time evolution of the phase-separated texture of DDA-9 at 145 °C: (b) $t = 10$ s; (c) $t = 60$ s; (d) $t = 200$ s; (e) $t = 600$ s; (f) $t = 1200$ s; (g) $t = 1800$ s; (h) $t = 3600$ s. t is the time spent after the T-drop. These micrographs are obtained from the same area of the same sample.

$$L(t) \sim t^{1/3} \tag{5}$$

toward the end of regime I, which is again consistent with the experimental result shown in Figure 2d. Here we should note the following point: the first three data points in the early stage of regime I in Figure 2c and d (obtained in the time scale of $t \leq 40$ s) have the values of R_I smaller than about 20 μm, and hence the droplets have 3D characteristics. This leads to a breakdown of the 2D approximation given by eqs 1 and 2 and also to less accurate determination of ρ_I and R_I. Thus, less weight should be put to the data in this early stage. Needless to say that approximate power laws given by eqs 4 and 5 show only qualitative tendencies in time evolution of the observed quantities but not definite scaling laws at all.

We propose here that the increase of $\rho_I(t)$ and the slowing down of the growth rate of R_I to the limiting growth rate are due to the chain segregation: the anisotropic matrix still contains an excess amount of low molecular weight chain species which lost extended-chain conformation at 148 °C and are unstable in a nematic medium; these chains involving a large packing free energy are gradually separated from the anisotropic matrix into the isotropic drops in regime I. The chain segregation eventually slows down and stops, giving rise to a saturation in $\rho_I(t)$ in the end of regime I. Hereafter the structure organization changes according to a diffusion−coalescence of isotropic droplets, giving rise to a decreasing number of ρ_I, increasing value of R_I or a decreasing value of L, and a constant value of x_I (the volume fraction of the two phases being conserved). Thus the system crosses over from a *nonconserved-order parameter system* (in which x_I is not conserved) to a *conserved-order parameter system*.

The chain segregation in regime I, leading to the increase in ρ_I, R_I, and x_I, lowers the bulk free energy of the system. On the other hand, it also increases the interfacial free energy accompanied by the increase of L with t. However, the cost of the interfacial free energy may be compensated by relaxation of the packing free energy of the low molecular weight species in the optically anisotropic medium. The chain segregation is manifested itself in our experimental results, i.e., in a slight variation in the retardation color and brightness of the anisotropic phase as shown in the micrographs of Figure 1b−d.

The coarsening mechanism in regime I is primarily controlled by the diffusion−condensation of small molecular weight species to isotropic drops through chain segregation. During the coarsening process in the late stage of regime I the drops grow in size, but their number stays approximately constant with time, as shown in Figure 2a. Moreover, the centers of mass of

large drops do not significantly shift with time, as indicated by the micrographs c and d in Figure 1 and some micrographs taken in between (not shown here). This aspect is highlighted in Figure 5 in which the time evolution of the images corresponding approximately to Figure 1c and d is given. The centers of mass of some large drops (appearing dark in Figure 5) from $t = 40$ to 100 s are indicated by white points in Figure 5a and they are superposed on the square grid in Figure 5b in which the centers are shown by black points. From Figure 5 we recognize that the centers of mass of large drops and their number do not change significantly in the late stage of regime I, except for the two drops coalesced into a larger one in the time period between 80 and 100 s (see drops marked by arrows). This observation implies chain segregation of low molecular weight species from the nematic phase and their incorporation into the isotropic drops (the diffusion−condensation process).

Regime II. In regime II, we speculate that the segregation of chain species into the isotropic and anisotropic phases according to their chain lengths stops and each phase has attained approximately compositional equilibrium with respect to the chain length distribution. As shown in Figure 2, the number-average density of drops decreases with time according to the power law with an exponent *approximately* equal to $-2/3$,

$$\rho_I(t) \sim t^{-2/3} \tag{6}$$

over the time scale covered in this experiment. However, the data in Figure 2a are not in excellent agreement with the scaling relation. This departure is possibly related to the finite size effect in the sampling area, because of the large drop size in regime II. Small drops coalesce into large ones at the near constant $x_I(t)$, $x_I(t) \sim t^0$, as shown in Figure 2c, indicating that the system becomes a conserved-order parameter system. The size $R_I(t)$ in regime II increases with time, according to a power law with an exponent approximately equal to $1/3$, as given by eq 3. The power law is consistent with the vaporization−condensation process proposed by Lifshitz−Slyozov[16] (LS process) or with the diffusion−coalescence process[14,15] involving the hydrodynamic interactions.[15,17] From eq 2 together with the results shown in Figure 2a and b, $L(t)$ should decrease with t according to

$$L(t) \sim t^{-1/3} \tag{7}$$

in regime II, which is again consistent with the experimental result shown in Figure 2d.

Following interesting features should be noted in regime II: (i) the shape of the isotropic drops is not a perfect circle, but an ellipse, in particular in the case when the distance between two adjacent drops is small; and (ii) the anisotropic networks traversing the isotropic phase have a catenoidal shape with a negative Gaussian curvature.[18] Feature i is shown in a series of ellipsoidal drops marked by 1−4, 5−8, and 9 and 10 in Figure 1d or 1−3 in Figure 1e, for example. The long axes of the deformed drops tend to assume a local parallel orientation. Feature ii is shown by the network marked by C in Figure 1f and g, for example. These features may reflect elastic deformations[19] and anisotropic flow behavior[20] of the anisotropic phase and/or a viscosity difference of the two liquid phases[21] which are encountered in the self-organization process.

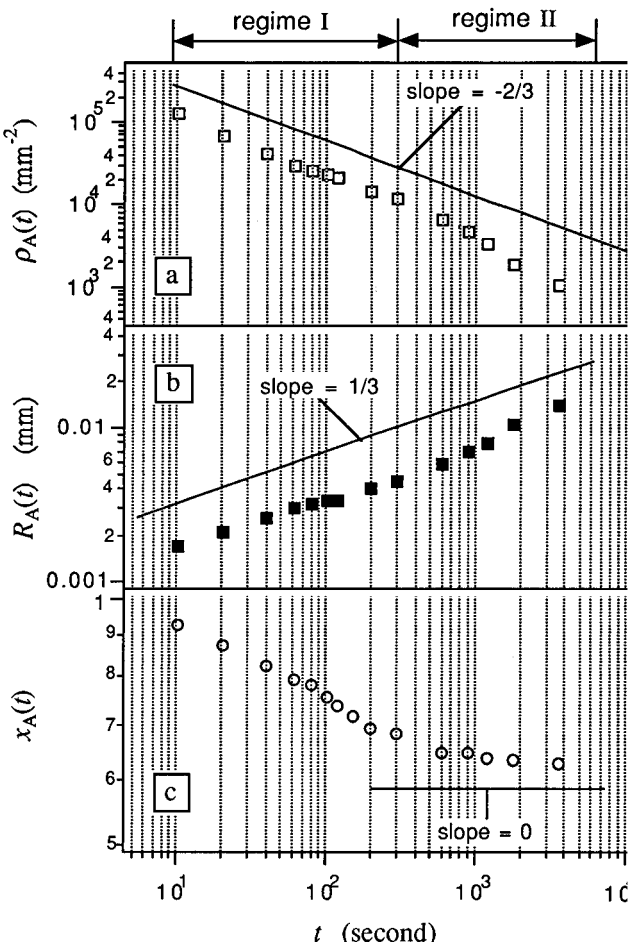

Figure 4. Plots of ρ_A, R_A, and x_A as a function of annealing time t. These quantities are determined from the micrographs, some of which are shown in Figure 3.

The two phases are expected to be co-continuous through the thinner parts of the catenoidal channels[18] of the anisotropic network, even though the characteristic size of the domains is greater than the film thickness and the structure has globally a two-dimensional character. A quasi-Poiseuille flow should occur, through the network having the catenoidal shape, from its center having a thinnest diameter to both sides of the network having larger diameters. This flow is driven by the capillary pressure and would orient the LC polymers and break the network up, as demonstrated by the broken network marked by B and Bf in Figure 1f. This leads to a coarsening of isotropic drops and of the anisotropic network. This process decreases the interface length, as shown in Figure 2d, and hence lowers the interfacial free energy. The flow driven by the capillary pressure results from the interfacial tension, and the coarsening of the phase-separating domains due to this interfacial tension effect was discussed by Siggia[22] for mixtures of isotropic liquids.

A stochastic nature of the network break is proposed here to be responsible for the self-similar growth of the network. The broken parts of the network having an excess interface curvature, as demonstrated by the parts of the network marked by B and Bf in Figure 1f, are absorbed in the network in such a way that the excess curvatures are relaxed, as shown by the change from Bf in Figure 1f to Bg in Figure 1g. This process is essentially identical to the process theoretically treated by Kawasaki for isotropic fluid mixtures.[23] Kawasaki's interface dynamics for conserved-order parameter sys-

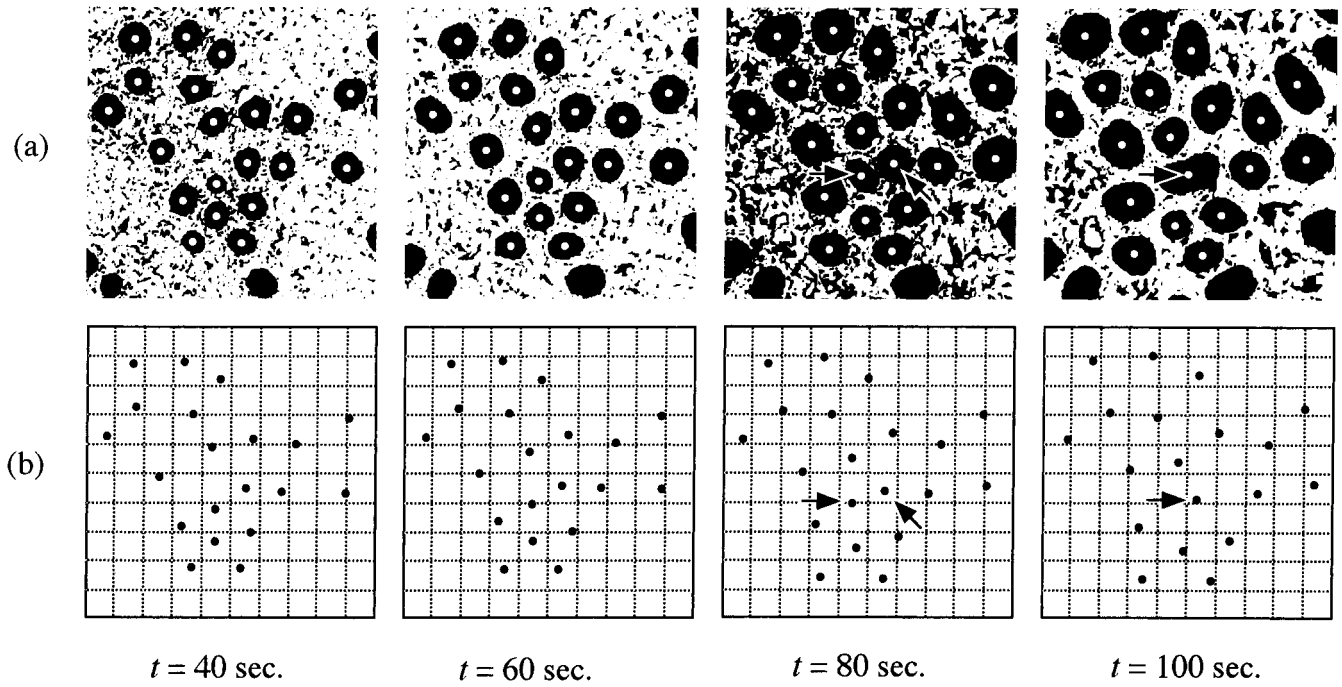

Figure 5. (a) Time evolution of the drops in the micrographs from t = 40 to 100 s. Centers of mass of some large drops are indicated by white points. (b) These centers in (a) are located on a square grid for easy spatial recognition.

tem without the hydrodynamic interactions predicts the time evolution of the characteristic length scale $\Lambda(t)$ as given by

$$\Lambda(t) \sim t^{1/3} \tag{8}$$

consistent with our result (eq 3). Thus the growth law (eq 3) found experimentally may reflect one or combinations of the following three mechanisms: the LS vaporization−condensation process (mechanism a), the diffusion−coalescence process in the fluid system[14,17,24] (i.e., with hydrodynamic interactions) (mechanism b) and Kawasaki's interface dynamics for the conserved-order parameter systems with the absence of the hydrodynamic interactions (mechanism c). It is crucial to point out that all these mechanisms are proposed for phase-separating mixtures composed of isotropic liquids. It is not straightforward as to whether the same mechanisms are applicable for mixtures with one component being liquid crystal. Although the scaling law of eq 3 is valid only for qualitative arguments, the exponent appears not to be affected by the fact that one phase is in the nematic liquid crystal state: only the prefactor might be affected by the liquid crystal characteristics. These intriguing points are deserved for future studies.

Finally we note that thick parts of the network have a polydomain texture as supported by the schlieren texture. The thinner parts have an oriented texture driven by the capillary flow. Thus the patterns are characterized by two kinds of order parameters: (i) the order parameter associated with the concentration fluctuations of the molecular species forming a liquid crystal phase and those forming an isotropic phase and (ii) orientation order parameters characterizing the texture of the LC phase.

B. Mechanisms of Self-Organization via Phase Separation Induced by a T-Drop. As we did before, the time evolution of the structure shown in Figure 3 may be divided into two regimes judging from the results shown in Figure 4: regime I at t < 300 s (the corresponding structure change being shown in micrographs a−d in Figure 3) and regime II at $t \geq$ 300 s (the corresponding one in the micrographs e−h in Figure 3).

Regime I. Figure 3b shows that when the specimen was quenched to 145 °C, a phase-separated texture composed of very many small anisotropic drops in the isotropic matrix was developed. These anisotropic drops seem to still contain low molecular weight species whose phase transition temperature is lower than 145 °C and which have lost the extended-chain conformation required for being incorporated into the nematic phase. The low molecular weight species are gradually expelled into the isotropic phase, as shown in the decreasing fraction of the anisotropic domains $x_A(t)$ with t in Figure 4c. This segregation process is expected to lower the bulk free energy of the system. Concurrently with the segregation process, the very small anisotropic drops surrounded by the isotropic matrix grow through a diffusion−coalescence process (Figure 4b), which lowers the interfacial free energy. This causes a decrease of the number of anisotropic drops $\rho_A(t)$ and an increase of the drop size $R_A(t)$, as shown Figure 4a and b, respectively. From Figure 4a and b we can see that in regime I the time evolution of ρ_A and R_A approximately obeys the power laws with exponents of about $-^2/_3$ and $^1/_3$, respectively, i.e.,

$$\rho_A(t) \sim t^{-2/3} \tag{9}$$

and

$$R_A(t) \sim t^{1/3} \tag{10}$$

although $x_A(t)$ does not reach the equilibrium value. These results show that the significant feature in regime I is a concurrence of the chain-segregation process and the diffusion−coalescence process of the anisotropic drops. This feature in the T-drop process is quite different from that in the T-jump process: in the T-jump process the chain segregation process dominates the

diffusion−coalescence process in regime I and the later becomes influential after stopping of the former in regime II.

Regime II. At $t \geq 300$ s (regime II), the chain segregation process is almost arrested and hence x_A reaches the equilibrium value, as shown in Figure 4c, but the diffusion−coalescence process of the anisotropic drops continues, as seen in Figures 3e and f and 4a and b. Large drops diffuse and coalesce to form finally large domains with an irregular shape, as shown in Figure 3g and h. The structure attained in the long-time limit (Figure 3h) is quite similar to that shown in Figure 1h.

From Figure 4a and b we can see that in regime II the time evolution of ρ_A and R_A also obeys approximately the power laws with exponents of about $-^2/_3$ and $^1/_3$, respectively, as shown by eqs 9 and 10. The conservation of volume (or area) fraction of the anisotropic phase $x_A(t) \sim \rho_A(t)R_A^2(t)$ is valid only in regime II where the segregation is arrested (cf. eq 1 for the T-jump process). This indicates that the coarsening mechanism in regime II is controlled by one of the following mechanisms or a combination thereof as in the case of the T-jump experiments: (a) vaporization−condensation model proposed by Lifshitz−Slyozov,[16] (b) diffusion−coalescence[14,24] of the drops in fluid mixtures (having hydrodynamic interactions[17]) and (c) interface dynamics for conserved-order parameter systems.[22] From Figure 4a and b, we can further see that at $t > 1000$ s the experimental data clearly deviate from the linear relations between log ρ_A and log t, and between log R_A and log t, showing a growth of the texture that is faster than predicted by eqs 9 and 10. This may be related to the formation of irregularly shaped and percolated domains in Figure 3g and h. This process may be explained by the mechanism c with its increasing hydrodynamic contribution with time.[17] Note that the interface dynamics for conserved-order parameter systems with full hydrodynamic interactions[17,23] predicts the growth

$$\Lambda(t) \sim t^1 \tag{11}$$

A similar trend appears to exist for the result shown in Figure 2 at $t \gtrsim 1000$ s.

C. Comparison of Self-Organization Mechanisms and Processes Occurring in T-Jump and T-Drop Processes. Although some comparisons have been already made in section B in Experimental Results and section B in the Discussion, it may be worthy to summarize the similarity and dissimilarity. The intermediate structures developed after the T-jump and T-drop processes are quite different: isotropic drops in an anisotropic matrix (Figure 1) vs anisotropic drops in an isotropic matrix (Figure 3). However, the two systems tend to form essentially identical structures in the final stage, as shown in Figures 1h and 3h, although these structures do not yet correspond to the equilibrium structure.

In both systems, the self-organization behavior can be divided into two regimes. In regime I the growth of drops due to the chain segregation and diffusion−coalescence generally occurs, although the chain segregation dominates the diffusion−coalescence in the self-organization induced by T-jump process, while the chain segregation and diffusion−coalescence concurrently occur in the self-organization induced by the T-drop process. The differences in the two processes were discussed in detail in sections A and B in the Discussion. In regime II, only the growth of drops occurs. The growth of drops in the two processes seems to obey the same scaling law (eqs 3 and 10), indicating that the coarsening mechanisms in both systems are similar. The changes from regime I to regime II for both the T-jump and T-drop experiments occur at $t \cong 300$ s. This may imply that the rate of chain segregation in both cases is the same or similar to each other. This in turn may imply that the mechanism of chain segregation for both cases is the same; i.e., the shorter chain species are expelled from the anisotropic phase.

In addition to the similarity and dissimilarity as pointed out above in the self-organization of the two systems, it is important to note that the average sizes of drops at a given time are quite different: $R_I(t) > R_A(t)$ as is clearly seen in Figures 2b and 4b. This means that the prefactor in the power law is different for the two systems. This dissimilarity may be due to a different viscosity of the matrix phase: the anisotropic matrix may have lower viscosity than the isotropic matrix. It may be also due to the different coalescence behavior between anisotropic and isotropic drops: in order for the two anisotropic drops to coalesce into single particles, the two particles at the coalesced portion must have a similar molecular orientation. The coalescence does not necessarily result in growth into a larger drop in the case of anisotropic drops, while it does in the case of isotropic drops.

Summary

In this paper we studied the self-organization mechanisms of two systems composed of isotropic drops in the anisotropic matrix and of anisotropic drops in the isotropic matrix in the biphase region of the same LC polyester through the T-jump and T-drop processes, respectively. In both systems, the phase separation and the self-organization of textures were divided into two regimes. In regime I, growth of drops due to chain segregation and diffusion−coalescence occurs and the volume fraction of one phase $x_A(t)$ changes with time, while in regime II, only the drop growth due to diffusion−coalescence takes place, keeping $x_A(t)$ constant (conserved-order parameter system). In regimes I and II, the growth of the drop-size R can be approximately scaled by the same power law $R(t) \sim t^{1/3}$, suggesting that the coarsening mechanism in both systems is similar. The growth law implies that the following mechanisms may occur: (a) Lifshitz−Slyozov's vaporization−condensation process; (b) the diffusion−coalescence process of the drops in fluid mixtures, and (c) Kawasaki's interface dynamics for conserved-order parameter systems. We note that the matrix viscosity and the coalescence behavior of anisotropic drops and isotropic drops are different for the two systems. However, these differences affect only the prefactors of the scaling laws on $R_I(t)$ or $R_A(t)$ with t. The final structure become similar for both systems.

Acknowledgment. W.W. gratefully acknowledges support by a scholarship for his postdoctoral research provided by the Japan Society for the Promotion of Science (ID93090). A part of this work was supported by Grants-in-aid for Encouragement of Young Scientist-A from the Ministry of Education, Science and Culture, Japan (00093090) and by a scientific grant from Polyplastics Co. Ltd., Japan. A.B. acknowledges the support of NSF Grant DMR-9201439.

References and Notes

(1) Stupp, S. I; Moore, J. S.; Martin, P. G. *Macromolecules* **1988**, *21*, 1228.

(2) Shiwaku, T.; Nakai, A.; Hasegawa, H.; Hashimoto, T. *Macromolecules* **1990**, *23*, 1590.
(3) Fredrickson, G. H.; Leibler, L. *Macromolecules* **1990**, *25*, 531.
(4) Blumstein, R. B.; Blumstein, A. *Mol. Cryst. Liq. Cryst.* **1988**, *165*, 361.
(5) Volino, F.; Allonneau, J. M.; Giroud-Godquin, A. M; Blumstein, R. B.; Stickles, E. M.; Blumstein, A. *Mol. Cryst. Liq, Cryst., Lett. Sect.* **1984**, *102*, 21.
(6) d'Allest, J. F.; Wu, P. P.; Volino, F.; Blumstein, A.; Blumstein, R. B. *Mol. Cryst. Liq, Cryst., Lett. Sect.* **1986**, *3*, 103.
(7) d'Allest, J. F.; Sixou, P.; Blumstein, A.; Blumstein, R. B. *Mol. Cryst. Liq. Cryst.* **1988**, *157*, 229.
(8) Kim, D. Y.; d'Allest, J. F.; Blumstein, A.; Blumstein, R. B. *Mol. Cryst. Liq. Cryst.* **1988**, *157*, 253.
(9) Esnault, P.; Gauthier, M. M.; Volino, F.; d'Allest, J. F.; Blumstein, R. B. *Mol. Cryst. Liq. Cryst.* **1988**, *157*, 273.
(10) Laus, M.; Caretti, D.; Angeloni, A. S.; Galli, G.; Chiellini, E. *Macromolecules* **1991,** *24*, 1459.
(11) Laus, M; Angeloni, A. S.; Galli, G.; Chiellini, E. *Macromolecules* **1992,** *25*, 5301.
(12) Nakai, A.; Wang, W.; Hashimoto, T.; Blumstein, A.; Maeda, Y. *Macromolecules* **1994**, *27*, 6963.
(13) Li, M. H.; Brûlet, A.; Keller, P.; Strazielle, C.; Cotton, J. P. *Macromolecules* **1993**, *26*, 119
(14) Binder, K.; Stauffer, D. *Phys. Rev. Lett.* **1974**, *33*, 1006.
(15) Hashimoto, T. In *Materials Science and Technology*; Cahn, R. W., Haasen, P., Kramer, E. J., Eds.; Vol. 12, *Structure and Properties of Polymers*; Thomas, E. L., Vol. Ed.;VCH: Weinheim, Germany, 1993; Chapter 6.
(16) Lifshitz, I. M.; Slyozov, V. V. *J. Phys. Chem. Solids* **1961**, *19*, 35.
(17) Kawasaki, K. *Prog. Theor. Phys.* **1977**, *57*, 826. Kawasaki, K.; Ohta, T. *Prog. Theor. Phys.* **1978**, *59*, 362.
(18) Hildebrandt, S.; Tromba, A. *Mathematics and Optimal Form*; Scientific American Library, Sci. Amer. Books, Inc: New York, 1985.
(19) Frank, F. C. *Discuss. Faraday Soc.* **1958**, *25*, 19.
(20) (a) Erickson, J. L. *Arch. Ration. Mech. Anal.* **1960**, *4*, 231; *Phys. Fluids* **1966**, *9*, 1205. (b) Leslie, F. M. *Q. J. Mech. Appl. Math.* **1966**, *19*, 357; *Arch. Ration. Mech. Anal.* **1968**, *28*, 265.
(21) Onuki, A. *Europhys. Lett.* **1994**, *28*, 175.
(22) Siggia, E. D. *Phys. Rev.* **1979**, *A20*, 595.
(23) Kawasaki, K. *Ann. Phys., N.Y.* **1984**, *154*, 319.
(24) Binder, K. *Phys. Rev.* **1977**, *B15*, 4425.

MA951116W